Spectroscopy of two-field Inflation

Welling, Y.M.

Orbital Inflation with ultra-light fields

In this chapter we present a class of inflationary models with two light fields that have predictions similar to those of single field inflation. Inflation proceeds along an 'angular' isometry direction in field space at arbitrary 'radius' and is a special case of Orbital Inflation discussed in Chapter 2. More precisely, we study the Orbital Inflation in the limit of vanishing entropy mass[1]. We dub this 'ultra-light Orbital Inflation', because it realizes the shift symmetry described in [138]. If the field radius of curvature of the inflationary trajectory is sufficiently small, the amplitude of isocurvature perturbations and primordial non-Gaussianities are highly suppressed. Ultra-light Orbital Inflation mimics single field inflation, because only one degree of freedom is responsible for the observed perturbations.

We study a toy model of ultra-light Orbital Inflation in § 3.2. This allows us to intuitively understand its interesting properties. In the successive sections we make our intuitive arguments more precise. In § 3.3 we derive the family of two-field models which allow for ultra-light Orbital Inflation and give the corresponding exact solutions. We prove neutral stability of ultra-light Orbital Inflation in § 3.4. Then, in § 3.5 we recap the definition of mass and the consequences of having massless isocurvature perturbations. Finally, we study the phenomenology of ultra-light Orbital Inflation in § 3.6.

The results in this chapter are based on joint work with Ana Achúcarro, Edmund Copeland, Oksana Iargyina, Gonzalo Palma and Dong-Gang Wang.

[1] The entropy mass is the effective mass of isocurvature perturbations. The definition of mass is non-trivial in a time-dependent inflationary background. By computing the normal modes of the coupled system of perturbations, we find a dispersion relation of the isocurvature perurbations corresponding to modes of mass μ as defined in Eq. 3.18. Therefore it is μ that we identify as the entropy mass. For more details, see § 2.2.3.

3.1 Introduction

The Planck data [115] reveal that inflationary perturbations are Gaussian and adiabatic to a high level of accuracy. A possible explanation for the observed simplicity is that the perturbations are generated by a single degree of freedom with small self-interactions. Do the observations therefore imply that, besides the inflaton, no other light fields are active during inflation? The answer is no. As pointed out in [138], in the limit that the other fields are massless, but coupled to the inflaton, the predictions mimic those of single field inflation.

Inflation with massless isocurvature modes behaves like single field inflation, because only one degree of freedom is relevant for the observed perturbations. The single field behavior is of dynamical origin. The key feature is that the isocurvature perturbations freeze out on superhorizon scales and constantly feed the curvature perturbations. Therefore, the isocurvature perturbations generate the temperature fluctuations we observe in the sky.

In this work we provide a realization of a family of two-field inflationary models in which the isocurvature perturbations become exactly massless (see footnote 1). We dub this ultra-light Orbital Inflation. We use the two-field generalization of the Hamilton-Jacobi formalism [74, 75, 77, 78] presented in Chapter 2 to derive the form of the potential. The key characteristic of *ultra-light* Orbital Inflation is that inflation proceeds along an isometry direction of the field metric at *arbitrary radius*. The resulting scalar field potential and kinetic term are given by

$$V = 3H^2M_p^2 - 2M_p^4\frac{H_\theta^2}{f(\rho)}, \quad 2K = f(\rho)\partial\theta^2 + \partial\rho^2 \ , \tag{3.1}$$

where the fields are denoted by θ and ρ. Moreover, the Hubble parameter H is a function of θ only and $f(\rho) > 0$.

In this chapter we point out several interesting properties of ultra-light Orbital Inflation:

- Each attractor is an *exact* solution to the highly non-linear system of field equations and Friedmann equation. This is ensured by using the Hamilton-Jacobi formalism.
- This system is neutrally stable. A small perturbation orthogonal to a given attractor solution will bring us to one of the neighboring attractors.
- Because isocurvature (= normal) perturbations move us freely between attractors, this implies that they are exactly massless. Thanks to the

Hubble friction their velocity decays and therefore their amplitude freezes out.

- The quadratic action of perturbations has enhanced symmetry. On top of the usual shift symmetry of curvature perturbations $\mathcal{R} \to \mathcal{R} + \text{const}$, the masslessness of the isocurvature perturbation $\mathcal{S}$ implies a combined shift symmetry [138]

$$\mathcal{S} \to \mathcal{S} + c, \quad \dot{\mathcal{R}} \to \dot{\mathcal{R}} - \lambda c. \tag{3.2}$$

  We show that we can understand this as a result of the background dynamics. The symmetry transformation is related to a map of one background attractor to another, labeled by the continuous parameter c.

- For large enough λ this implies that curvature perturbations are dynamically enhanced and the predictions of the power spectra coincide with those of single field inflation [138]. Moreover, the final curvature perturbations are completely determined by the initial isocurvature perturbations. Therefore, these multi-field inflation scenarios mimic the predictions of single-field inflation.

We work in Planck units $\hbar = c = 1$ and the reduced Planck mass is given by $M_p = (8\pi G)^{-1/2}$.

3.2 A toy model with neutrally stable orbits

To illustrate the idea, we consider a simple toy model in flat field space in polar field coordinates $\phi^a = (\theta,\ \rho)$. The kinetic term and potential are given by

$$K = \frac{1}{2}\left(\rho^2(\partial\theta)^2 + (\partial\rho)^2\right), \quad V = \frac{1}{2}m^2 M_p^2\left(\theta^2 - \frac{2M_p^2}{3\rho^2}\right) \tag{3.3}$$

This potential allows for orbital solutions with a constant angular velocity, see Figure 3.1. It explicitly breaks the shift symmetry of θ to overcome the Hubble friction. Moreover the ρ-dependent part of the potential provides a centripetal force that stabilizes the radial direction. Although the potential in this toy model is unbounded from below, inflation only takes place in the physically consistent regime where the potential energy is positive. Moreover, our analysis is restricted to radii $\rho > M_p$. Therefore, we only care about the local form of the potential close to the inflationary trajectory, which we assume is captured well by this toy potential. The full true potential should be well-behaved at smaller radii.

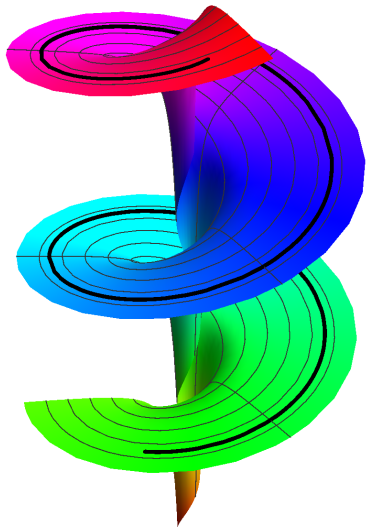

Figuur 3.1: The potential given in Eq. 3.3 together with a typical inflationary trajectory. The black line corresponds to the full numerical solution.

3.2.1 Exact solution

We start with an analysis of the homogeneous background dynamics of $\theta(t)$ and $\rho(t)$. The field equations of motion and the Friedmann equation read

$$\rho^2\ddot{\theta} + 3H\rho^2\dot{\theta} + 2\rho\dot{\rho}\dot{\theta} + m^2M_p^2\theta = 0, \tag{3.4a}$$

$$\ddot{\rho} + 3H\dot{\rho} - \rho\dot{\theta}^2 + \frac{2m^2M_p^4}{3\rho^3} = 0, \tag{3.4b}$$

$$6H^2M_p^2 = \rho^2\dot{\theta}^2 + \dot{\rho}^2 + m^2M_p^2\left(\theta^2 - \frac{2M_p^2}{3\rho^2}\right). \tag{3.4c}$$

Typically, it is very hard to find exact solutions to such a system of equations, because they are highly non-linear. In particular the friction terms in the

field equations involve the square root of the right-hand side of the Friedmann equation Eq. 3.4c. In this case, however, the system allows for *exact* stable solutions of the form

$$\rho = \rho_0, \quad \dot{\theta} = \pm\sqrt{\frac{2}{3}}\frac{mM_p^2}{\rho_0^2}, \quad H^2 = \frac{m^2\theta^2}{6}, \quad \epsilon = \frac{2M_p^2}{\rho_0^2\theta^2}, \tag{3.5}$$

for any ρ_0. Here $\epsilon \equiv -\frac{\dot{H}}{H^2}$ is the slow roll parameter that measures the deviation from the de Sitter solution. Notice that the negative contribution to the squared Hubble parameter H^2 from the radial part of the potential is precisely cancelled by the angular kinetic energy. We will show neutral stability of these exact solutions in § 3.4. Therefore, in what follows we can assume the inflationary trajectory to be one of them.

3.2.2 Symmetry transformation and massless modes

The inflationary trajectory proceeds along an isometry of the field metric, namely the angular direction. This is clearly not a geodesic in flat field space. The radius of curvature of the trajectory is constant and given by $\kappa = \rho_0$. From Eq. 3.5 we can deduce $\left(\theta^2\right)' = \frac{2\theta\dot{\theta}}{H} = -\frac{4M_p^2}{\rho_0^2}$, where the prime denotes a derivative with respect to efolds $(..)' = \frac{d}{dN}(..)$. Given some reference attractor, this implies that we can label each attractor by a continuous parameter c with the corresponding map

$$\rho_c = \rho_0 + cM_p, \quad \left(\theta_c^2\right)' = \frac{\left(\theta_0^2\right)'}{(1 + cM_p/\kappa)^2}, \tag{3.6}$$

This transformation identifies all attractors. Without loss of generality we take θ_0' to be negative. Let's figure out what this mapping tells us about the behavior of quantum fluctuations.

In the flat gauge, the isocurvature perturbations $\mathcal{S}$ are associated with $\delta\rho/M_p$ and the curvature perturbations $\mathcal{R}$ with $\frac{\rho}{\sqrt{2\epsilon}M_p}\delta\theta$. Using Eq. 3.5 we can rewrite this as $\mathcal{R} = \frac{\rho_0^2}{4M_p^2}\delta(\theta^2)$, which implies $\delta(\theta^2)' = \frac{4M_p^2}{\rho_0^2}\mathcal{R}' = -\left(\theta_0^2\right)'\mathcal{R}$. We aim to find the action of the transformation on the perturbations. For that purpose we split $\rho = \rho_0 + \mathcal{S}M_p$ and $\left(\theta^2\right)' = \left(\theta_0^2\right)'(1 - \mathcal{R}')$. We next determine how a small c changes $\mathcal{S}$ and $\mathcal{R}'$. In the long wavelength limit every transformed set of perturbations $(\mathcal{S}_c, \mathcal{R}_c')$ should provide a new solution to the equations of motion. This is because homogeneous perturbations map background solutions onto each other. Therefore, going back to cosmic time,

we expect to find the following *symmetry* for linearized perturbations

$$\mathcal{S} \to \mathcal{S} + c, \quad \dot{\mathcal{R}} \to \dot{\mathcal{R}} + \frac{2HM_p}{\kappa}c. \tag{3.7}$$

We will confirm this in § 3.2.3. Furthermore, we expect the isocurvature perturbations to be massless, as a consequence of the shift symmetry of $\mathcal{S}$.

3.2.3 Power spectrum and single field behavior

To get an intuitive notion of the behavior of perturbations, we employ the δN formalism [74, 220–223], see also Figure 3.2. First, we integrate the attractor equation for θ in Eq. 3.5 by changing time t to efolds $dN = Hdt$:

$$N = \frac{\rho^2}{4M_p^2}\theta^2 - \frac{1}{2}, \tag{3.8}$$

with N the number of efolds until the end of inflation (defined by $\epsilon_{\text{end}} = 1$). In the δN formalism, one computes the time evolution of a fluctuation for a given wavenumber k_* from horizon crossing $k_* \sim a_* H_*$ until the end of inflation, by treating it as a homogeneous fluctuation. Therefore, we can simply perturb equation Eq. 3.8 and the curvature perturbation at the end of inflation is given by

$$\mathcal{R}(k_*) = \delta N_* \approx \frac{1}{\sqrt{2\epsilon}M_p}(\rho\delta\theta)_* + \frac{2N_* + 1}{\kappa}\delta\rho_*. \tag{3.9}$$

Remember that the radius of curvature in our toy model is given by $\kappa = \rho_0$. The initial perturbations $(\rho\delta\theta)_*$ and $\delta\rho_*$ are random variables that arise from quantum fluctuations with typical amplitude $\frac{H_*}{2\pi}$ at horizon crossing. Neglecting their initial cross-correlation we find the following spectrum of curvature perturbations

$$P_{\mathcal{R}}(k_*) \approx \frac{H_*^2}{4\pi^2 M_p^2}\left(\frac{1}{2\epsilon_*} + \frac{4N_*^2 M_p^2}{\kappa^2}\right). \tag{3.10}$$

We confirm this result in § 3.5 and compare with the *Planck* data in § 3.6.

In the limit of 'small' radius of curvature, i.e.

$$1 \leq \frac{\kappa^2}{M_p^2} \ll 8\epsilon_* N_*^2 \approx 4N_*, \tag{3.11}$$

the second term in Eq. 3.10 dominates and the final power spectrum is determined by the isocurvature perturbations. The lower bound comes from assuming the validity of our simple computation, see § 2.3. Moreover, since

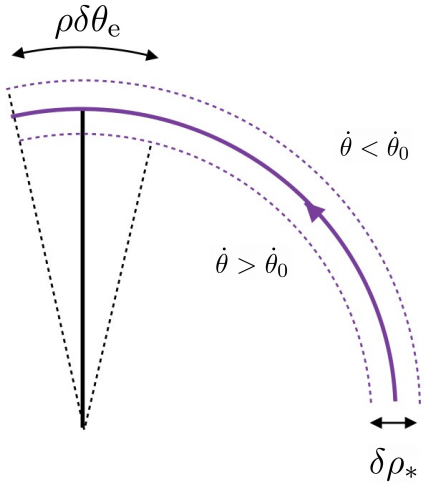

Figuur 3.2: Visualization of the growth of curvature perturbations along the inflationary trajectory. The inflationary trajectory corresponds to the solid purple line and proceeds in the angular direction. In the δN formalism, we consider the effect of an initial constant perturbation $\delta\rho_*$ at the time of horizon crossing on the duration of inflation. The perturbed trajectory proceeds in the angular direction as well, but has smaller or larger radius of curvature (lower and upper purple dashed segment, respectively). The corresponding orbital velocity $\rho\dot\theta$ is larger for the lower curve, therefore inflation ends earlier compared to the background trajectory. On the other hand inflation ends later on the upper curve. This results in nonzero fluctuations in the curvature perturbations $\mathcal{R} = \delta N \sim \rho\delta\theta_{\rm e}$. The amplitude of curvature fluctuations keeps growing after horizon crossing until the end of inflation. Moreover, the smaller the radius of curvature of the trajectory, the larger the final amplitude of curvature perturbations.

the isocurvature perturbations have a constant amplitude, they will be dynamically suppressed with respect to the curvature perturbations

$$\frac{P_{\mathcal{S}}}{2\epsilon P_{\mathcal{R}}} = \frac{1}{1+\frac{4M_p^2}{\kappa^2}N_*} \ll 1 \ . \tag{3.12}$$

Hence, at the linear level we recover single field predictions. This happens because the final spectrum is generated by a single degree of freedom, namely the isocurvature perturbation. Therefore, this two-field model of inflation behaves like single-field inflation.

Finally, we estimate the amplitude of the bispectrum using the δN forma-

lism. In the limit of small radius of curvature Eq. 3.11, we find

$$f_{NL}^{\delta N} \approx \frac{5}{6}\frac{N_{\rho\rho}}{N_\rho^2} = \frac{5}{6}\epsilon_* \ . \tag{3.13}$$

It is slow roll suppressed. Therefore, the phenomenology is very similar to that of single field inflation. To understand whether these models obey the consistency relation $f_{NL} = \frac{5}{12}(1 - n_s)$ in the squeezed limit, we also need to compute the intrinsic bispectrum. We present the full in-in computation of the bispectrum in [224]. This will tell us if these models are distinguishable from single field inflation.

3.3 Ultra-light Orbital inflation

In this section we derive a general family of two-field models that admit ultra-light Orbital Inflation. The defining feature of ultra-light Orbital Inflation is that inflation proceeds along an isometry direction of the field metric at *arbitrary radius*. Therefore, we can follow the same derivation as Orbital Inflation presented in § 2.4.2 based on the Hamilton-Jacobi formalism [74, 75, 77, 78]. However, the difference is that we have to assume that the Hamilton-Jacobi equation Eq. 2.44 and constraint equation Eq. 2.46 are satisfied *globally*, or at least for a finite range of values of ρ.

The two equations we should solve simultaneously are the Hamilton-Jacobi equation Eq. 2.44 and constraint equation Eq. 2.46. Using Eq. 2.49 they simplify to

$$3H^2M_p^2 = V + 2M_p^4\frac{H_\theta^2}{f} \ , \tag{3.14a}$$

$$3HH_\rho - 2M_p^2\frac{H_\theta H_{\rho\theta}}{f(\rho)} \ , \tag{3.14b}$$

for *any* value of ρ. The constraint equation implies that H has to be a function of θ only. Assuming the opposite, namely that $H_\rho \neq 0$ for *some* value of ρ, we can rewrite the constraint as

$$(\ln H)_\theta(\ln H_\rho)_\theta = \frac{3f}{2M_p^2}. \tag{3.15}$$

Since the right hand side is independent of θ, we can only allow for a solution of the form $(\ln H)_\theta \sim g(\theta)$ and $(\ln H_\rho)_\theta \sim \frac{1}{g(\theta)}$, which is impossible to solve. We conclude that H does not depend on ρ.

Therefore, we conclude that a two-field inflationary model of the form

$$V = 3H^2M_p^2 - 2M_p^4\frac{H_\theta^2}{f(\rho)}, \quad G_{ab} = \begin{pmatrix} f(\rho) & 0 \\ 0 & 1 \end{pmatrix} \tag{3.16}$$

with $H = H(\theta)$, admits ultra-light Orbital Inflation. The background dynamics of ultra-light Orbital Inflation is governed by Eq. 2.49:

$$T^a = \frac{1}{\sqrt{f}}(-1,\ 0) \quad \text{and} \quad N^a = (0,1) \quad (\text{because } \dot\rho = 0), \tag{3.17a}$$

$$\dot\theta = -2M_p^2\frac{H_\theta}{f}, \quad \epsilon = \frac{2M_p^2H_\theta^2}{fH^2}, \quad \kappa = \frac{2f}{\partial_\rho f}, \quad \mathbb{R} = \frac{2}{\kappa^2} - \frac{f_{\rho\rho}}{f}. \tag{3.17b}$$

3.3.1 Symmetry argument and massless isocurvature perturbations

As alluded to in the introduction, in ultra-light Orbital Inflation we expect the isocurvature perturbations to be massless (see footnote 1). Their effective mass is indeed zero

$$\mu^2 = V_{NN} + \epsilon H^2M_p^2\left(\mathbb{R} + \frac{6}{\kappa^2}\right) = 0\ . \tag{3.18}$$

The first term is the standard Hessian term plus geometrical corrections $V_{NN} \equiv N^aN^b\left(V_{ab} - \Gamma^c_{ab}V_c\right)$. The effective mass μ receives centrifugal and geometrical corrections, because the inflationary background solution is time-dependent. For ultra-light Orbital Inflation we have $V_{NN} = V_{\rho\rho}$. Using the properties of the inflationary background solution Eq. 3.17 we find that the three terms cancel exactly.

The background dynamics hints about the existence of a shift symmetry for perturbations. Like we argued for the toy model in § 3.2.2, the map Eq. 3.6 that relates all background trajectories is generalized to

$$\rho_c = \rho_0 + cM_p, \quad (G(\theta_c))' = (G(\theta_0))'\frac{f(\rho_0)}{f(\rho_0 + cM_p)}. \tag{3.19}$$

Here $G(\theta)$ is the primitive of $G_\theta = \frac{H}{H_\theta}$. Moreover, in the flat gauge we can write $\mathcal{R} = \sqrt{\frac{f(\rho)}{2\epsilon M_p^2}}\delta\theta = \frac{f(\rho)}{2M_p^2}\delta G$. This implies $\delta G' = -G_0'\mathcal{R}$. We Taylor expand the transformation of the angular velocity for small $\frac{cM_pf_\rho}{f} = \frac{2cM_p}{\kappa}$ to linear order. This yields $G_c' = G_0'\left(1 - \frac{2cM_p}{\kappa}\right)$. Therefore, the same arguments as in

§ 3.2.2 apply and we are led to expect the combined shift symmetry of linear perturbations

$$\mathcal{S} \to \mathcal{S} + c, \quad \dot{\mathcal{R}} \to \dot{\mathcal{R}} + \frac{2HM_p}{\kappa}c. \tag{3.20}$$

We confirm our intuition in § 3.5.

3.4 Stability

Our results rely on the fact that the inflationary trajectory is one of the exact solutions, which we said was an attractor. We now demonstrate neutral stability of the exact solutions.

What do we mean exactly with neutral stability in our dynamical system? We have seen that there is a continuous set of orbital solutions parametrized by ρ_0. Moreover, we said that normal perturbations move us freely between these 'attractors', so the system is clearly not stable in the usual sense. The property we need to prove is that small perturbations shift us to another inflationary solution $\dot{\rho} = 0$.

Each attractor solution Eq. 3.17 corresponds to a point in the $(\dot{\rho}, \dot{\theta})$ plane. Unfortunately, these points are all different and lie on a curve. Moreover, we prefer to do the stability analysis in efolds rather than time, since we expect the Hubble friction to play a crucial role. Therefore, we introduce the variables

$$x(\theta, \rho, \theta', \rho') \equiv \frac{fH}{M_p^2 H_\theta}\theta' - 2\frac{f}{f_\rho}\frac{\rho'}{M_p^2} + 2, \tag{3.21a}$$

$$y(\theta, \rho, \theta', \rho') \equiv \frac{fH}{M_p^2 H_\theta}\theta' + 2\ , \tag{3.21b}$$

$$z(\theta, \rho) \equiv \frac{fH^2}{M_p^2 H_\theta^2} - 2/3 \tag{3.21c}$$

Here a prime denotes a derivative with respect to efolds $(..)' = \frac{d}{dN}(..)$. Remember that $H = H(\theta)$ and $f = f(\rho)$. Our definition of stability now amounts to the presence of a fixed point at $(x, y) = (0, 0)$.

We choose these specific variables, because it turns out that the stability of this system is non-trivial to prove analytically. If we simply perturb the field equations we will find zero eigenvalues associated with the perturbations that move us between attractors. Moreover, it is not obvious how to find variables such that the linearized system of perturbations becomes diagonal.

The definition of x and y above are based on an observation for the models where the Hubble parameter is linear in θ. For $H \sim \theta$ the potential in Eq. 3.16 satisfies the following scaling relation

$$\theta V_\theta - 2\frac{f}{f_\rho} V_\rho = 2V. \tag{3.22}$$

This ensures that the equations for x and y diagonalize at the linear level. This we can use to prove linear stability for the models $H \sim \theta$, which we show in Eq. 3.4.1. In fact it turns out to apply to any power law $H \sim \theta^n$. Moreover, we argue that neutral stability also applies to more general models.

3.4.1 Linear stability analysis

The first step is to rewrite the field equations and second Friedmann equation in terms of the x, y, ρ and z variables. The equations of motion read

$$x' + (3-\epsilon)x + \left(2\left(\frac{f}{f_\rho}\right)_\rho - g(\theta)\right)\left(\frac{\rho'}{M_p}\right)^2 + \frac{2(z+2/3)}{z} g(\theta)\,(\epsilon - \epsilon_0) = 0,$$

$$y' + (3-\epsilon)y + \frac{2}{z}\left(-\frac{1}{3}\left(\frac{\rho'}{M_p}\right)^2 - \frac{1}{2}y^2 + 2y\right) - g(\theta)\left(\frac{\rho'}{M_p}\right)^2 + \frac{2(z+2/3)}{z} g(\theta)\,(\epsilon - \epsilon_0) = 0,$$

$$z' = 2(y-2)\,(1-g(\theta)) + \left(\frac{M_p f_\rho}{f}\right)^2 \frac{y-x}{2}\left(z + \frac{2}{3}\right),$$

$$\frac{\rho'}{M_p} = \frac{M_p f_\rho}{f}\frac{y-x}{2},$$

$$\epsilon = \frac{1}{2}\frac{(y-2)^2}{z+2/3} + \frac{M_p^2 f_\rho^2}{f^2}\frac{(x-y)^2}{8},$$

where $\epsilon_0 = \frac{2}{z+2/3}$. All the terms in brackets are combined to be manifestly zero on the attractor. We introduced the model specific function $g(\theta) \equiv \frac{H H_{\theta\theta}}{H_\theta^2}$. Note that $g(\theta)$ is in general a function of z and ρ, but it reduces to a constant in the case when we have a power law $H(\theta) \sim \theta^n$, and it is zero for $n = 1$.

In terms of the four variables, ultra-light Orbital Inflation is given by $(x, y, z', \rho') = (0, 0, -4(1-g(\theta)), 0)$, and we would like to prove that this is the attractor solution. It will be sufficient to show that $(y, \rho') = (0, 0)$ is a fixed point. Note that the friction term is very large during inflation. We can already see that, without the friction, the system would be unstable. Let's figure out if the friction is large enough to render the system stable.

To study the stability of the point $(y, \rho') = (0, 0)$, we linearly perturb the

equations around the desired attractor with $\epsilon = \frac{2}{z+2/3}$. We get

$$\delta x' + \left(3 - \frac{2}{z+2/3}\right)\delta x - \frac{4g(\theta)}{z}\delta y = 0, \tag{3.24a}$$

$$\delta y' + \left(3 - \frac{2}{z+2/3} + \frac{4(1-g(\theta))}{z}\right)\delta y = 0, \tag{3.24b}$$

$$\delta z' = 2(1-g(\theta))\delta y + \left(\frac{M_p f_\rho}{f}\right)^2 \frac{\delta y - \delta x}{2}\left(z + \frac{2}{3}\right), \tag{3.24c}$$

$$\frac{\delta\rho'}{M_p} = \frac{M_p f_\rho}{f}\frac{\delta y - \delta x}{2}. \tag{3.24d}$$

Surprisingly, the linearized system of perturbations is very simple for any $g(\theta)$. In particular, for constant $g(\theta)$ we can can explicitly prove stability. We show this in a moment in Eq. 3.4.1. For a more general function we have to express $g(\theta)$ in terms of z and ρ and integrate the equations numerically. However, inspection by eye suggests that generically we may expect the system to be stable. If $(1 - g(\theta))$ takes values of order 1 and does not vary too rapidly, then z will take large values during inflation and behave smoothly as well. In that case we see from Eq. 3.24a and Eq. 3.24b that $\delta x'$ and $\delta y'$ are dominated by the friction terms $-3\delta x$ and $-3\delta y$ respectively. Therefore, we expect both of them to decay like e^{-3N}. Finally Eq. 3.24d then implies that we quickly converge to the fixed point.

Power law inflation $H \sim \theta^n$

In the case of power law inflation with $1 - g(\theta) = \frac{1}{n}$ we can integrate the δy equation Eq. 3.24b, using $z = z_0 - \frac{4}{n}N$. This we can then use to solve for δx as well. We find the following solution

$$\delta y = \delta y_0 \frac{z}{z_0}\left(\frac{2+3z_0}{2+3z}\right)^{n/2} e^{-3N}, \tag{3.25a}$$

$$\delta x = \delta x_0 \left(\frac{2+3z_0}{2+3z}\right)^{n/2} e^{-3N} + \delta y_0 \frac{4(n-1)N}{n}\left(\frac{2+3z_0}{2+3z}\right)^{n/2} e^{-3N}. \tag{3.25b}$$

Plugging these solutions back into Eq. 3.24d we conclude that $(y, \rho') = (0, 0)$ is a fixed point. This proves stability for power law inflation.

3.5 Inflation with massless isocurvature perturbations

In this section we recap the relevant results from the linear perturbations analysis in two-field inflation. In particular, we focus on the limit that the isocurvature perturbations are massless [138] (see footnote 1).

3.5.1 Quadratic action of perturbations

The full action of our two-field models of inflation has the general form

$$S = \frac{1}{2}\int d^4x\sqrt{-g}\left[M_p^2 R - G_{ab}\partial\phi^a\partial\phi^b - 2V(\phi^a)\right] \ . \tag{3.26}$$

with the field metric and potential from Eq. 3.16. We study the dynamics of linearized perturbations around the exact homogeneous inflationary background solution.

In the flat gauge, the scalar metric perturbation is set to zero. The comoving curvature perturbation $\mathcal{R}$ is then given by the projection of the field perturbation along the inflationary trajectory: $\mathcal{R} = \frac{1}{\sqrt{2\epsilon}M_p}T_a\delta\phi^a$. The isocurvature perturbation $\mathcal{S}$ corresponds to the remaining orthogonal field perturbation to the inflationary trajectory: $\mathcal{S} = \frac{N_a\delta\phi^a}{M_p}$. The quadratic action for perturbations takes the following form

$$S^{(2)} = \frac{1}{2}\int d^4x a^3 M_p^2\left[2\epsilon\left(\dot{\mathcal{R}} - \frac{2HM_p}{\kappa}\mathcal{S}\right)^2 + \dot{\mathcal{S}}^2 - \mu^2\mathcal{S}^2 + ..\right] \tag{3.27}$$

The ellipses denote the gradient terms $-(\partial_i\mathcal{S})^2 - 2\epsilon(\partial_i\mathcal{R})^2$. The perturbations are combined in such a way that the entropy mass μ is manifest (see footnote 1).

3.5.2 Massless isocurvature modes and symmetry

In the limit of $\mu^2 = 0$, the quadratic action Eq. 3.27 enjoys a combined shift symmetry [138]

$$\mathcal{S} \to \mathcal{S} + c, \quad \text{and} \quad \dot{\mathcal{R}} \to \dot{\mathcal{R}} + \frac{2HM_p}{\kappa}c. \tag{3.28}$$

The combined shift symmetry is exactly as we argued from the background dynamics in § 3.3.1 !

3.5.3 Power spectrum and effective single field behavior

The power spectra of perturbations in the massless limit can be well estimated from the coupled evolution of perturbations on superhorizon scales. The full derivation relies on an in-in computation to account for the coupled evolution of perturbations on subhorizon scales [138]. This gives the same results up to subleading corrections.

When $\mu = 0$, the linearized system of coupled perturbations simplify in the superhorizon limit. The isocurvature perturbation quickly converges to a constant on superhorizon scales where it sources the curvature perturbation. The final dimensionless power spectrum of curvature perturbations in the massless limit is given by (see § 2.3)

$$P_{\mathcal{R}} = \frac{H^2}{8\pi^2\epsilon_*}\left(1 + 2\epsilon_*\left(\int dN\ \frac{2M_p}{\kappa}\right)^2\right). \tag{3.29}$$

Note that the power spectrum is completely determined by the isocurvature perturbations if the radius of curvature κ is sufficiently small:

$$2\epsilon_*\left(\int dN\ \frac{2M_p}{\kappa}\right)^2 \gg 1 \tag{3.30}$$

Using this condition, the spectrum of isocurvature perturbations will be dynamically suppressed as well

$$\frac{P_{\mathcal{S}}}{2\epsilon P_{\mathcal{R}}} \approx \left(2\epsilon_* \int dN\ \frac{2M_p}{\kappa}\right)^{-2} \ll 1\ . \tag{3.31}$$

We confirm all intuitive results for the toy model in § 3.2.3 .

Summarizing, two-field inflation with massless isocurvature perturbations, together with a trajectory of sufficiently small radius of curvature mimics the predictions of single field inflation at the level of the power spectra.

3.6 Phenomenology

We now turn to the predictions for the spectral tilt n_s and the tensor-to-scalar ratio r. In this section we use the result from § 3.5 for the power spectrum in the limit that the isocurvature perturbations are massless and the radius of curvature of the trajectory is constant:

$$P_{\mathcal{R}} = \frac{H^2}{8\pi^2\epsilon_*}\left(1 + 2\epsilon_*\left(\frac{2M_p}{\kappa}\right)^2 N_*^2\right). \tag{3.32}$$

During ultra-light Orbital Inflation we can use this expression, since $\kappa = \frac{2f}{\partial_\rho f}$ is constant on the trajectory.

The spectral tilt and tensor-to-scalar ratio are (to good approximation) given by

$$n_s = \frac{\partial \ln P_{\mathcal{R}}}{\partial N}, \tag{3.33a}$$

$$r = \frac{16\epsilon_*}{\left(1 + \frac{8\epsilon_* M_p^2}{\kappa^2} N_*^2\right)}, \tag{3.33b}$$

where we have to be careful to use $\frac{\partial N_*}{\partial N} = -1$, since N_* counts the number of efolds backwards. The predictions depend on the function $H(\theta)$. Like in single field slow roll inflation, this function determines how ϵ and η scale with N_*.

For concreteness, we consider power law inflation $H \sim \theta^p$. Using the exact solution of ultra-light Orbital Inflation Eq. 3.17, we integrate the equation of motion for θ and plug it back in the expression for ϵ to find

$$\epsilon_* = \frac{p}{2N_* + p}, \quad \eta_* \equiv \frac{\epsilon_*'}{\epsilon_*} = \frac{2}{2N_* + p} \ . \tag{3.34}$$

Note that these are exactly the same slow-roll parameters as the single field models $V \sim \varphi^{2p} - \frac{2}{3}$ (see § 1.2.3), which also have the exact homogeneous attractor solution $\dot{\phi} = -2pM_p^2\phi^{p-1}$. Using Eq. 3.33b, the predictions for n_s and r are therefore well approximated by

$$n_s \approx 1 - \frac{p+1}{N_*} - \frac{4p}{\frac{\kappa^2}{M_p^2} + 4pN_*}, \tag{3.35a}$$

$$r \approx \frac{8p\kappa^2}{N_*\kappa^2 + 4pM_p^2 N_*^2} \ . \tag{3.35b}$$

We plot these analytical predictions against the Planck 1σ and 2σ contours [115] in Figure 3.3. The radius of curvature κ^2/M_p^2 varies between 1 and 10^5. Moreover, we take N_* between 50 and 60. Our toy model from § 3.2 corresponds to the purple contour and resembles the predictions of chaotic inflation when $\kappa \to \infty$. Furthermore, we show the predictions of linear inflation (red contour) and $\phi^{2/3}$ inflation (orange contour).

The first thing to notice is that our results for n_s and r only depend on the value of κ and are therefore insensitive to the details of the field metric. We might expect that the higher order correlation functions retain this information. We estimate the amplitude of the bispectrum in the δN formalism like

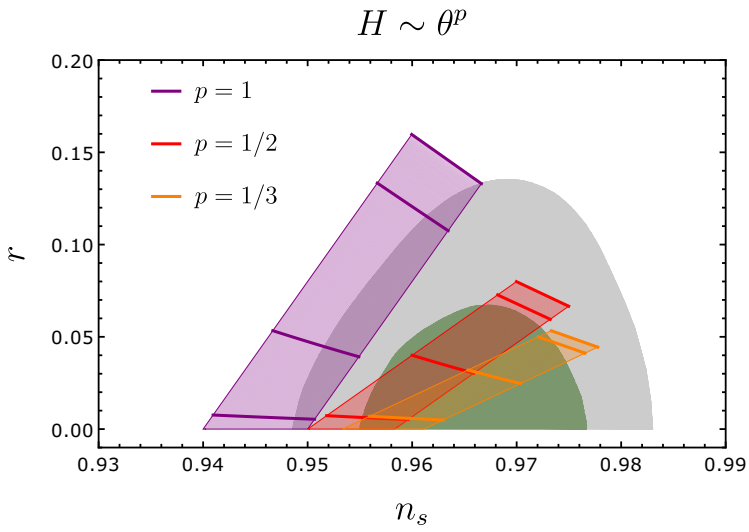

Figuur 3.3: The analytical predictions Eq. 3.35 for (n_s, r) compared to the *Planck* 1σ and 2σ contours [115]. The colors of the contours correspond to different values of p, which determines the scaling of the Hubble parameter $H \sim \theta^p$. The slow roll parameters are exactly as those of a single field model with potential $V \sim \theta^{2p} - \frac{2}{3}$. We show the predictions for wavenumbers which cross the horizon $50 - 60$ efolds before the end of inflation. The predictions for (n_s, r) depend on the value of the radius of curvature κ of the inflationary trajectory. We vary κ^2/M_p^2 between 1 and 10^5, and indicate the values $(10, 10^2, 10^3, 10^5)$ with thick lines (from bottom to top).

we did in § 3.2.3, which gives

$$f_{NL}^{\delta N} \approx \frac{5}{6}\frac{\epsilon_*}{p}\left(1 - \frac{\kappa^2 \mathbb{R}}{2}\right) . \tag{3.36}$$

Here we assumed the limit of 'small' radius of curvature $\kappa^2 \ll \frac{2p^2}{\epsilon} M_p^2$. We see that the bispectrum has the potential to distinguish between different field spaces through its dependence on the Ricci scalar $\mathbb{R}$. We need a full in-in computation of the bispectrum [224] to verify this result.

Coming back to the predictions for n_s and r, we find they are pushed downwards and to the left in the (n_s, r) plane as the radius of curvature decreases. Therefore, in the case of power law inflation only for small p the predictions remain within the *Planck* contours. However, we saw in Chapter 2 that the predictions are sensitive to the value of μ^2/H^2. In particular, if a small mass is generated, we arrive at a different conclusion.